

## Research Paper

# Improvement of Solenoid Valve Performance by Axial Slots Inserted in the Armature

Robert GORAJ

Paul Gossen Str. 99, 91052 Erlangen, Germany  
e-mail: robertgoraj@gmx.de

The article presents numerical investigations of the influence of axial slots inserted in the armature of a solenoid valve (SV) on the magnetic and frictional force acting on the armature during its movement. The numerical computations were performed using the method of finite differences. The computational room of the magnetic solution was the radial air gap of a SV. In the case of the fluid mechanical solution the computation room was the oil film. Both of these rooms were functions of the circumferential position of the armature. These computational rooms were transformed to the co-ordinate system in each they get a rectangle. This transformation was performed by means of the Laplace operator derived using a function shoal and the differential geometry. The computed distributions of magnetic energy density in the radial air gap and the magnitude of the magnetic flux density on the side surface of the eccentrically positioned armature in the magnet yoke were presented and discussed. These distributions in the case of both slotted and non-slotted armature were visualised in the transformed co-ordinate systems and compared to one another. Also the distribution of the oil velocity in the oil film and the distribution of the shear stress vector at two different temperatures were shown in figures.

**Key words:** solenoid valve, armature, air gap, magnetic permeance.

### 1. INTRODUCTION

Modern design of SVs uses sophisticated analytical and numerical computation methods for better understanding and the improvement of their magnetic, fluid mechanical and thermal behaviour. In [1] an analytic formula for the estimation of the inductive power caused by the pulse width modulation of the coil current was derived. The inductive power was used as an input to the thermal calculation having an objective to estimate the time dependent temperature distribution in the armature of the SV. For SVs in each the armature can be position eccentrically in the sleeve, investigations of the existent eccentricity have been reported very rarely in the literature. In most studies on SVs the thickness of the radial gap is kept constant independent from the circumferential angle. In other words, researchers take an assumption that the armature is placed concentrically in the sleeve. This assumption implies the homogeneously distribution of

radial magnetic forces over the armature circumference. In order to include the effect of the armature eccentricity in the technical design, suitable computation methods are requested. One of these methods presented in [2] considers a mathematical way of transforming the geometry of the radial air gap into rectangular computation domain. The Laplace operator derived in [2] can be used for precise and time efficient numerical computations using the finite differences method. The objective of such computations is the estimation the transversal component of the magnetic force acting on the armature of SVs as well as the magnetic permeance of the radial air gap. The derived Laplace operator can be also used in fluid mechanical computations in order to estimate the velocity distribution in the oil film and viscous shear forces acting on the armature during its movement. The use of these algorithms allows performing computational investigations of the influence of proposed constructional changes of SVs. Some of these changes have the focus of the reduction of the transverse force by an introduction of segmentation in the armature member [3]. Other construction ideas try to minimize the transversal force by the insertion of small radial slots in the armature side surface [4]. In the literature one can find reports regarding investigations about finite difference approaches [5], simulations [6] and thermal influences [7] of SV. However, one cannot find hitherto any reports approaching the question, on what is the impact of the insertion of axial slots in the SV armature. This is mainly due to the fact that the idea [4] describes a relatively novel concept which was not investigated so far. The insertion, which is the subject of the present study, improves the performance of SVs especially at low operating temperatures and reduces frictional wear. In the investigated case the number of armature slots was set to ten. This number of armature slots was chosen in a random manner. The presented numerical investigation of the influence of armature slots has an objective to give a computational proof that there is at least one number of slots for which the performance of the considered SV can be increased. The idea protected by the patent [4] bases on a hypothetical assumption, that slots having a relatively small depth reduce viscous friction without significant worsening of the electromagnetic performance. This thesis ought to be verified using both computational methods and measurements. However, before starting a complex optimisation process including the number, the depth and the peripheral length of the slots, it is advisable to deliver in the very first research step some basic evidence of the potential of the idea [4].

## 2. DEFINITION OF THE PROBLEM

The simplified layout of the investigated SV shown in Fig. 1 consists of the following parts: (1) room filled with oil, (2) sleeve, (3) coil, (4) armature, (5) rod, (6) magnet core, (7) plunger, (8) magnet yoke, (9) axial holes. Both the

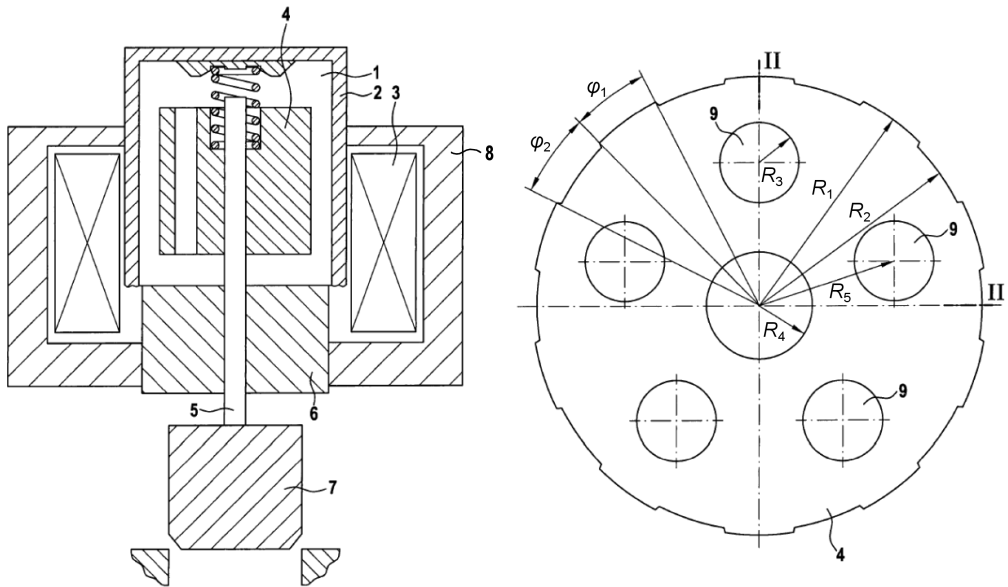


FIG. 1. Simplified layout of the SV (left) and the cross section of the armature [4].

oil and the material of the sleeve have the magnetic permeability equal to the permeability of the vacuum. The outer side of the sleeve and the inner side of the magnet yoke have same radii.

The armature has on its circumference some axial slots (shown in Fig. 1 on the right) heaving the depth of:

$$(2.1) \quad \delta = R_1 - R_2.$$

The aim of the investigation is to determine the impact of these slots on the forces acting on the armature. The investigation is restricted only to magnetic force and both viscous and dry friction force. Furthermore, both the number of the slots and their peripheral length defining by the ratio  $\varphi_2/\varphi_1$  were kept constant. In order to calculate these forces the outer contour of the armature was defined by the function  $\zeta$  shown in Fig. 2. In the considered SV the armature is not positioned concentrically in the sleeve by it is shifted toward the sleeve of the value  $e$ .

The local thickness of the oil film  $h_h$  or the local value of the air gap  $h_m$  was demonstrated symbolically by the function  $h$ . The distance  $\zeta + h_h$  indicates the inner side of the sleeve and the distance  $\zeta + h_m$  indicates the inner side of the magnet yoke. The room between the armature and the inner side of the sleeve or between the armature and the inner side of the magnet yoke is the computational room  $\Omega$  in which the distribution of the oil velocity or the

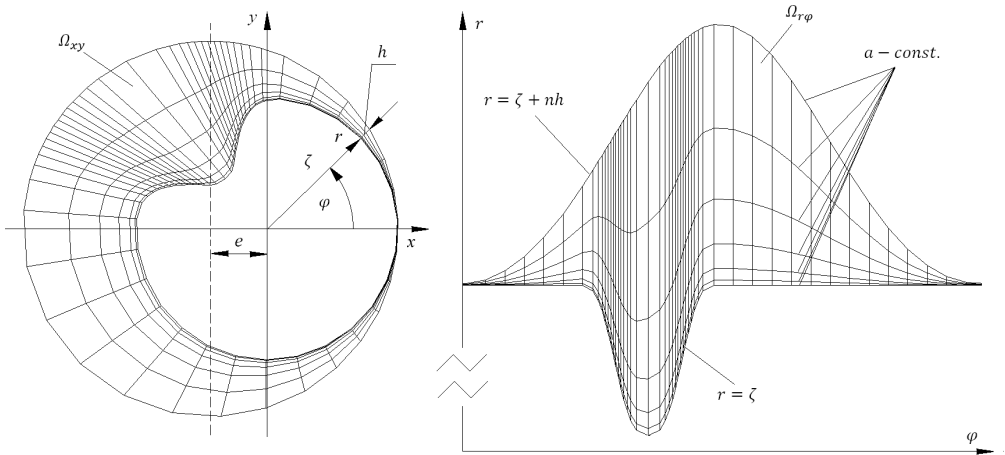


FIG. 2. Examples of a meshed computational room in different co-ordinate systems (left [11]).

distribution of magnetic field is to be determined. The position  $r$  inside the computation room  $\Omega_{r,\varphi}$  is scaled with the function  $n$  that takes the value “zero” on the armature contour and the value “one” on the inner side of the sleeve or the inner side of the magnet yoke.

### 3. VALVE OPERATION PRINCIPLE

Figure 3 shows a simplified layout of a solenoid valve. The armature (2) of the switching valve has the length  $L_h$ . It is located in the oil (6) oil having

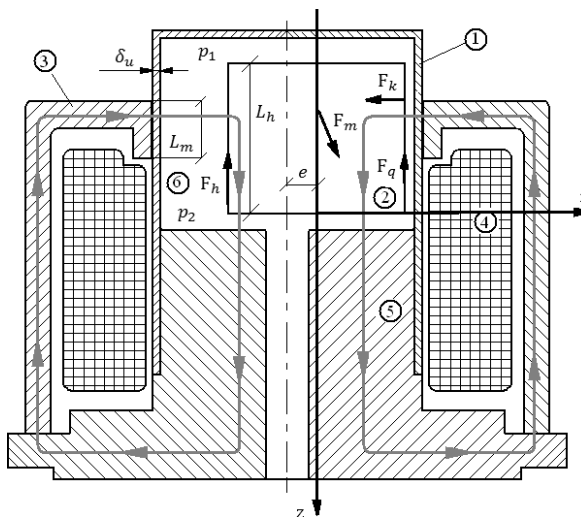


FIG. 3. Simplified layout of a 2/2 solenoid valve ([2], with small modifications).

the temperature  $T$ . Its  $z$ -axis is shifted from the  $z$ -axis of the sleeve (1) by the distance  $e$ . This offset is defined as the armature eccentricity.

In the coil (4) flows a constant electric current, which causes the magnetic field. The lines of the magnetic field extend through the sleeve, the radial air gap, the armature, the axial air gap, the magnetic core (5) and the housing (3). The length of the axial air gap  $h_b$  equals to the distance from (5) to (2). The length of the yoke pole equals  $L_m$ . Since the sleeve of the control valve is made of a paramagnetic material (aluminum alloy), the radial air gap consists of the thickness of the sleeve  $\delta_u$  and the radial clearance between the armature and the sleeve. The magnetic field causes the magnetic force  $\mathbf{F}_m$ . The axial component of this force sets the armature in motion. It moves in the  $z$ -direction with the constant velocity  $\mathbf{u} = u_0(T)\mathbf{e}_z$ . The armature movement arises a pressure drop in the oil equal  $p_2 - p_1$ . The radial component of the magnetic force is in equilibrium with the contact force  $\mathbf{F}_k$ . During the armature movement the viscous share  $\mathbf{F}_h$  acts on the armature.

#### 4. DIFFERENTIAL OPERATORS AND VECTOR SURFACE ELEMENT

Remarks: In this section vectors and tensors, as it is common in the differential geometry which is widely spread e. g. in the relativistic mechanics, are not marked using bold writings. Derivatives of scalar functions are written using the indexing, for example  $\partial h / \partial \varphi$  and  $\partial^2 h / \partial \varphi^2$  are written shortly by  $h_\varphi$  and  $h_{\varphi\varphi}$ . Similar indexing is used for components of tensors – see e.g. the metric tensor  $g_{ij}$  in the Euclidean space. Furthermore, computation domains in both orthogonal and curvilinear co-ordinate system are marked using the same indexing.

In order to find forces acting on the armature a calculation model was built and solved numerically using the method of finite differences. As it will be show in the next section this model was used to solve the Poisson's differential equation. The co-ordinate system in which calculations were performed is the  $a, \alpha$  co-ordinate system. In this co-ordinate system the computation domain specified by the region  $\Omega_{r\varphi}$  (Fig. 2 on the right) gets the rectangle  $\Omega_{a\alpha}$  shown in Fig. 4.

The transformation from the polar co-ordinate system  $r, \varphi$  to the  $a, \alpha$  co-ordinate system was performed using the transformation (4.1), (4.2):

$$(4.1) \quad n(a) = h(\varphi)^{-1} (r - \zeta(\varphi)),$$

$$(4.2) \quad \alpha = \alpha(\varphi).$$

In the co-ordinate system  $a, \alpha$  the distance from the armature contour to the inner side of the sleeve or to the inner side of magnet yoke is kept constant in each circumferential position. This discretizing method is a relatively novel

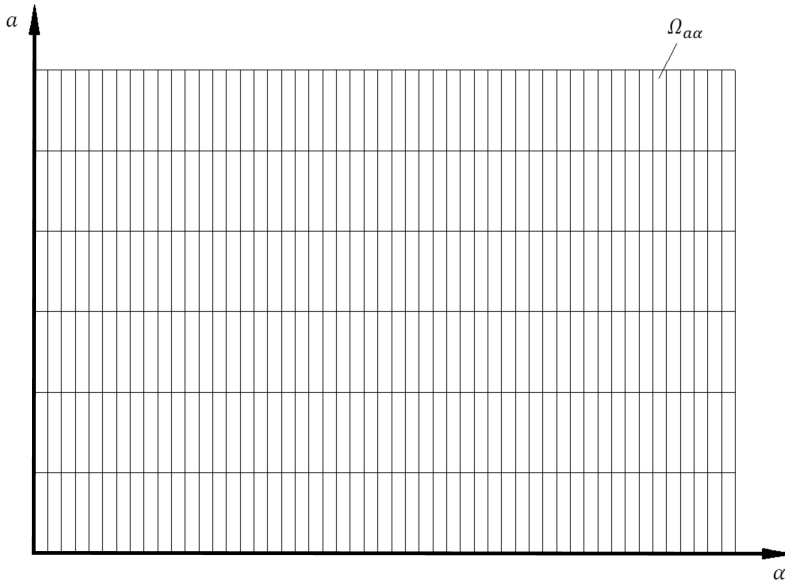


FIG. 4. Meshed computation domain of the Poisson's differential equation in  $a$ ,  $\alpha$  co-ordinate system [11].

computation method [2, 8]. It has this advantage in comparison to the Finite Element Method (FEM) that regions with small magnetic or hydraulic gap in which both magnetic flux density and viscous shear stress are the highest can be automatically mesh more densely than regions with big gaps. This method of discretizing allows an increase of computation precision with a simultaneous reduction of the mesh node numbers. The method bases upon the idea of introducing a curvilinear co-ordinate system in each the computational domain gets a rectangle. In order to find the Laplace operator in this co-ordinate system the most general definition of this operator – the Laplace-Beltrami operator was used. The Laplace-Beltrami operator of a scalar function  $V$  in any co-ordinate system can be expressed using the Einstein notation widely spread in the differential geometry [8–10]:

$$(4.3) \quad \nabla_i \nabla^i V = \frac{1}{\sqrt{g}} \partial_i (\sqrt{g} g^{ij} \partial_j V).$$

$g^{ij}$  in (4.3) is the contravariant metric tensor of the second rank. One can find its general covariant form by [10]:

$$(4.4) \quad g_{ij} = \frac{\partial X^k}{\partial q^i} \frac{\partial X^k}{\partial q^j}.$$

The  $k$  in (4.4) is the summation index. The position vector  $X$  is defined as:

$$(4.5) \quad X = (n(a)h(\varphi) + \zeta(\varphi)) e^r + z e^z.$$

The derivatives of the position vector (4.5) are:

$$(4.6) \quad X_a = n_a h e^r,$$

$$(4.7) \quad X_\alpha = \alpha_\varphi^{-1} \begin{pmatrix} (nh_\varphi + \zeta_\varphi) \cos \varphi - (nh + \zeta) \sin \varphi \\ (nh_\varphi + \zeta_\varphi) \sin \varphi + (nh + \zeta) \cos \varphi \\ 0 \end{pmatrix},$$

$$(4.8) \quad X_z = e^z.$$

The use of (4.4) gives the components of the covariant metric tensors:

$$(4.9) \quad g_{11} = (n_a h)^2,$$

$$(4.10) \quad g_{12} = \frac{nh_\varphi + \zeta_\varphi}{\alpha_\varphi} n_a h,$$

$$(4.11) \quad g_{21} = g_{12},$$

$$(4.12) \quad g_{22} = \frac{(nh_\varphi + \zeta_\varphi)^2 + (nh + \zeta)^2}{\alpha_\varphi^2}.$$

The determinant of the metric tensors is equal:

$$(4.13) \quad g = \frac{(n_a h)^2 (nh + \zeta)^2}{\alpha_\varphi^2}.$$

The contravariant metric tensor is defined as [8]:

$$(4.14) \quad g^{ij} = g_{ij}^{-1}.$$

The components of the metric tensor in the contravariant form are [11]:

$$(4.15) \quad g^{11} = \frac{1}{(n_a h)^2} + \left( \frac{nh_\varphi + \zeta_\varphi}{n_a h (nh + \zeta)} \right)^2,$$

$$(4.16) \quad g^{12} = -\alpha_\varphi \frac{nh_\varphi + \zeta_\varphi}{n_a h (nh + \zeta)^2},$$

$$(4.17) \quad g^{21} = g^{12},$$

$$(4.18) \quad g^{22} = \frac{\alpha_\varphi^2}{(nh + \zeta)^2}.$$

The Laplace-Beltrami operator simplifies in the considered case to:

$$(4.19) \quad \Delta = (\partial_a (\sqrt{g}g^{11}) + \partial_\alpha (\sqrt{g}g^{21})) \frac{\partial_a}{\sqrt{g}} + (\partial_\alpha (\sqrt{g}g^{22}) + \partial_a (\sqrt{g}g^{12})) \frac{\partial_\alpha}{\sqrt{g}} + g^{11}\partial_{aa} + g^{22}\partial_{\alpha\alpha} + 2g^{12}\partial_{a\alpha}.$$

Performing of all differentiations needed in (4.19) yields the Laplace operator on the 2-d basis [2, 11]:

$$(4.20) \quad \Delta = \frac{\alpha_{\varphi\varphi}}{(nh + \zeta)^2} \partial_\alpha + \left( \frac{1}{(nh + \zeta)n_a h} - \frac{n_{aa}}{h^2 n_a^3} + 2 \frac{nh_\varphi + \zeta_\varphi}{n_a h^2 (nh + \zeta)^2} h_\varphi - \frac{(nh_\varphi + \zeta_\varphi)^2 n_{aa}}{h^2 n_a^3 (nh + \zeta)^2} - \frac{nh_{\varphi\varphi} + \zeta_{\varphi\varphi}}{n_a h (nh + \zeta)^2} \right) \partial_a + \left( \frac{1}{(n_a h)^2} + \left( \frac{nh_\varphi + \zeta_\varphi}{n_a h (nh + \zeta)} \right)^2 \right) \partial_{aa} + \frac{\alpha_\varphi^2}{(nh + \zeta)^2} \partial_{\alpha\alpha} - 2\alpha_\varphi \frac{nh_\varphi + \zeta_\varphi}{n_a h (nh + \zeta)^2} \partial_{a\alpha}.$$

The obtained Laplace operator (4.20) is identical to the one derived in [2] using another mathematical way – namely a shoal of differential functions. The further differential operator need for the computation of magnetic and fluid mechanical forces is the nabla operator. According to [9] the gradient of a scalar function  $V$  in any co-ordinate system is a covariant vector defined as:

$$(4.21) \quad (\nabla V)_i = g^{ik} \frac{\partial X}{\partial q^i} \frac{\partial V}{\partial q^k}.$$

The derivatives of the position vector (4.5) are given by (4.6) to (4.7). With the use of the new basis with unit vectors:

$$(4.22) \quad e^a = e^r,$$

$$(4.23) \quad e^\alpha = \left( r^2 + (nh_\varphi + \zeta_\varphi)^2 \right)^{-1/2} \left( (nh_\varphi + \zeta_\varphi) e^r + r e^\varphi \right) \alpha_\varphi$$

and with the use of (4.1) one obtains the nabla operator [11]:

$$(4.24) \quad \nabla = \frac{e^a}{r^2} \left( \frac{r^2 + (nh_\varphi + \zeta_\varphi)^2}{r_a} \partial_a - \alpha_\varphi (nh_\varphi + \zeta_\varphi) \partial_\alpha \right) + \frac{e^\alpha}{r^2} \sqrt{r^2 + (nh_\varphi + \zeta_\varphi)^2} \left( \alpha_\varphi \partial_\alpha - \frac{(nh_\varphi + \zeta_\varphi)}{r_a} \partial_a \right).$$

According to [2] the operator nabla (4.24) can also be written on the  $r, \varphi$  basis in the compacter way:

$$(4.25) \quad \nabla = \frac{e^r}{n_a h} \partial_a + \frac{e^\varphi}{\zeta + nh} \left( \alpha_\varphi \partial_\alpha - \frac{\zeta_\varphi + nh_\varphi}{n_a h} \partial_a \right).$$

The last vector needed in further computations is the vector surface element. It can be obtained from the cross product of partial derivatives of (4.5) in  $\alpha$  and  $z$  direction:

$$(4.26) \quad dA = (X_\alpha \times X_z) d\alpha dz.$$

Setting (4.7) and (4.8) in (4.26) one obtains for any  $a$ -const the vector surface element [11]:

$$(4.27) \quad dA = \alpha_\varphi^{-1} ((\zeta + nh)e^r - (\zeta_\varphi + nh_\varphi)e^\varphi)_{a=0} d\alpha dz.$$

## 5. FINITE DIFFERENCES MODEL

After assuming a constant magnetic permeability of each component of the SV and neglecting the influence of the eddy current the magnetic field density  $\mathbf{B}$  existing in the domain  $\Omega_{a\alpha}$  can be represented by the gradient filed according to [12]:

$$(5.1) \quad \mathbf{B} = \mu_0 \nabla \psi.$$

The parameter  $\mu_0$  in (5.1) is the magnetic permeability of the vacuum. The function  $\psi$  is the scalar potential of the magnetic field intensity. After the use of the Gauss's law [13] the divergence of the magnetic field density is equal zero and one obtains the Laplace differential equation being the special case of the Poisson's differential equation:

$$(5.2) \quad \Delta \psi = 0.$$

For the solution to the Eq. (5.2) the Laplace operator (4.20) on the  $a, \alpha$  - basis was used. The function  $h$  in (4.20) was replaced with the circumference dependent length of the air gap  $h_m$ . Also the derivatives  $\partial h / \partial \varphi$  and  $\partial^2 h / \partial \varphi^2$  (written in the previous section shortly  $h_\varphi$  and  $h_{\varphi\varphi}$ ) were replaced with  $\partial h_m / \partial \varphi$  and  $\partial^2 h_m / \partial \varphi^2$ . The variables  $a, \alpha$  have the range of  $a \in [0, 1]$ ,  $\alpha \in [0, 2\pi]$ . On the  $a, \alpha$  - basis one can defined the armature contour by the vector  $Q_1 = (a = 0, \alpha)^T$  and the inner side of the magnet yoke by the vector  $Q_2 = (a = 1, \alpha)^T$ . In the case of the armature positioned concentrically in the magnet yoke the vector

$Q_2$  transformed to the  $r, \varphi$  - basis gets:  $Q_2 = (\delta_m, \varphi)^T$ . The parameter  $\delta_m$  in this vector is the thickness of the radial air gap. The boundary conditions of (5.2) are:

$$(5.3) \quad \psi(0, \alpha) = 0,$$

$$(5.4) \quad \psi(1, \alpha) = \theta_2.$$

The parameter  $\theta_2$  in (5.4) is the drop of the magnetomotive force in the domain  $\Omega_{xy}$ . It can be found using the Hopkinson's law [14]:

$$(5.5) \quad \theta_2 = \theta G_1 (G_1 + G_2)^{-1}.$$

The parameter  $\theta$  in (5.5) is the total drop of the magnetomotive force in the SV. It was assumed that in the considered system  $\theta$  stays constant. The parameter  $G_2$  in (5.5) is the permeances of the domain  $\Omega_{xy}$ , which was computed using [15]:

$$(5.6) \quad G_2 = \theta_2^{-1} \mu_0 \oint\!\!\!\!\!\oint_A (\nabla\psi)_{n=0} \cdot (d\mathbf{A})_{n=0}.$$

The nabla operator used in (5.6) was taken from (4.25) and the vector surface  $\mathbf{A}$  from (4.27). The integration was performed in the range  $\varphi \in [0, 2\pi]$ ,  $z \in [0, L_m]$ . The parameter  $L_m$  is the width of the yoke pole. Comparing (5.4) and (5.6) one can see that the permeance  $G_2$  is independent from  $\theta_2$ . That means, that in the computation of (5.2) one can use for the condition (5.4) any drop of the magnetomotive force satisfying the constrain:  $\theta_2 \in \mathcal{R}_+$  (e.g.,  $\theta_2 = 1$  [A]). The obtained fictive scalar potential must then be scaled by the relation (5.5). The parameter  $G_1$  in (5.5) is the permeance of the axial air gap, which was computed using [16]:

$$(5.7) \quad G_1 = \mu_0 A_d h_b^{-1}.$$

The parameter  $A_d$  in (5.7) is the area of the armature cross section. It was computed numerically using the triangle integration method and under consideration of the radii  $R_3$  and  $R_4$  shown in Fig. 1. After knowing the permeances of the radial and the axial magnetic gaps the distribution of the magnetic energy density in the radial air gap was found using [14]:

$$(5.8) \quad p_m = 2^{-1} \mu_0 |\nabla\psi|^2.$$

In the last step the electromagnetic force acting on the armature was computed [14]:

$$(5.9) \quad \mathbf{F}_m = F_m^x \mathbf{e}^x + F_m^y \mathbf{e}^y + F_m^z \mathbf{e}^z \\ = \iint_A p_m(n=0)(d\mathbf{A})_{n=0} + \frac{\mu_0}{2} \left( \frac{\theta}{h_b} \frac{G_2}{G_1 + G_2} \right)^2 A_d \mathbf{e}^z.$$

The transversal component of the electromagnetic force must stay in equilibrium with the contact force armature-sleeve. The reaction contact force  $\mathbf{F}_k$  was calculated by:

$$(5.10) \quad \mathbf{F}_k = F_k^x \mathbf{e}^x + F_k^y \mathbf{e}^y = - \iint_A p_k(d\mathbf{A})_{n=0}.$$

The function  $p_k$  in (5.10) is the distribution of the contact pressure calculated using the Greenwood-Williamson model [17]:

$$(5.11) \quad p_k = \pi \frac{16}{15} \sqrt{2} (m_R \beta \sigma)^2 E' \sqrt{\frac{\sigma}{\beta}} 3.48 \cdot 10^{-5} \left( 4 - \frac{h_h}{\sigma} \right)^{7.05} (1 - \varkappa).$$

The number of contact peaks per surface unit  $m_R$ , the curvature radius  $\beta$  of contact peaks and the roughness  $\sigma$  aren't independent from each other. It can be assumed that  $m_R \beta \sigma = 0.5$  [18]. The physical quantity  $E'$  is the reduced module of elasticity of the contact armature-sleeve. The function  $\varkappa$  is the Heaviside's function with the argument  $h_h(4\sigma)^{-1}$ . The integration (5.10) was performed in the range  $\varphi \in [0, 2\pi]$ ,  $z \in [0, L_h]$ . The parameter  $L_h$  is the axial length of the armature. Both the contact force and the magnetic force depend on the eccentricity of the armature. In the case of  $x$ -axis symmetric contour of the radial air gap and the oil film the force components  $F_k^y$  and  $F_m^y$  are equal zero. In this case the armature eccentricity can be obtained by the solving of the equation:

$$(5.12) \quad F_m^x(e) + F_k^x(e) = 0.$$

In this symmetric case the dry friction force can be obtained multiplying  $F_k^x$  by the friction coefficient  $\mu_q$  of the contact armature-sleeve according to:

$$(5.13) \quad \mathbf{F}_q = F_q^z \mathbf{e}^z = \mu_q F_k^x \mathbf{e}^z.$$

In the next computation step the oil velocity  $\mathbf{u}$  in the domain  $\Omega_{xy}$  (Fig. 2) was estimated using the stationery Navier-Stokes differential equation [19]:

$$(5.14) \quad \mathbf{f} - \rho^{-1} \nabla p + \nu \Delta \mathbf{u} + 3^{-1} \nu \nabla (\nabla \cdot \mathbf{u}) = 0.$$

The vector function  $\mathbf{f}$  in (5.14) are the mass forces,  $\rho$  is the oil density,  $p$  is the pressure and  $\nu$  is the kinematic viscosity of the oil. After having neglected the mass force and assuming the constant oil density and constant pressure drop the equation (5.14) simplifies in the case of the axial armature movement to [20]:

$$(5.15) \quad \Delta u^z = (p_2 - p_1)(\eta L_h)^{-1}.$$

The parameter  $\eta$  in (5.15) is the dynamic oil viscosity. The Laplace operator used in (5.15) was taken again from (4.20). This time however the function  $h$  in (4.20) was replaced with the circumference dependent oil film thickness  $h_h$ . Also the derivatives  $h_\varphi$  and  $h_{\varphi\varphi}$  were replaced with  $\partial h_h / \partial \varphi$  and  $\partial^2 h_h / \partial \varphi^2$ . This time the vector  $Q_2 = (a = 1, \alpha)^T$  defines the inner side of the sleeve. In the case of the armature positioned concentrically in the sleeve the vector  $Q_2$  transformed to the  $r, \varphi$  - basis gets:  $Q_2 = (\delta_h, \varphi)^T$ . The parameter  $\delta_h$  is the clearance armature-sleeve. The boundary conditions to (5.15) are:

$$(5.16) \quad u^z(0, \alpha) = u_0,$$

$$(5.17) \quad u^z(1, \alpha) = 0.$$

The parameter  $u_0$  in (5.16) is the axial velocity of the armature. After having solved (5.15) the viscous shear stress vector  $\boldsymbol{\tau}$  on the armature side surface was computed according to [21]:

$$(5.18) \quad \boldsymbol{\tau} = \eta \nabla u^z|_{n=0}.$$

The nabla operator in (5.18) was taken again from (4.25). The viscous friction force was computed using the integration of the viscous shear stress vector (5.18) over the armature side surface according to:

$$(5.19) \quad \mathbf{F}_h = F_h^z \mathbf{e}^z = \mathbf{e}^z \oint\!\!\!\!\!\oint_A \boldsymbol{\tau} \cdot (d\mathbf{A})_{n=0}.$$

The integration as in the case of the contact force was performed in the range  $\varphi \in [0, 2\pi]$ ,  $z \in [0, L_h]$ .

## 6. COMPUTATION RESULTS

A first numerical computation was performed in the case of non-slotted armature for the parameters listed in the Table 1. The computed distributions of magnetic energy density in radial air gap and the axial component of the oil velocity were evaluated on the  $a, \alpha$  - basis.

**Table 1.** Computation parameters.

Parameter	Value	Unit
$2R_1$	11.5	mm
$L_m$	3	mm
$L_h$	10	mm
$\delta_m$	300	$\mu\text{m}$
$\delta_h$	10	$\mu\text{m}$
$G_1$	228.4	nVs/A
$\theta$	600	A
$p_2 - p_1$	0.1	MPa
$T^{\min}, T^{\max}$	-10, 140	$^{\circ}\text{C}$
$\eta(T^{\min}), \eta(T^{\max})$	1.022, 0.0058	Ns/m <sup>2</sup>
$u_0(T^{\min}), u_0(T^{\max})$	0.25, 0.50	m/s

By solving the Eq. (5.12) one obtained the armature eccentricity of  $e = 8.535$  [mm]. The density of the magnetic energy in the radial air gap in the case of no-slotted armature varies from approximately 0.25 [MPa] to approximately 0.3 [MPa] in the whole computation range (see Fig. 5 on the left).

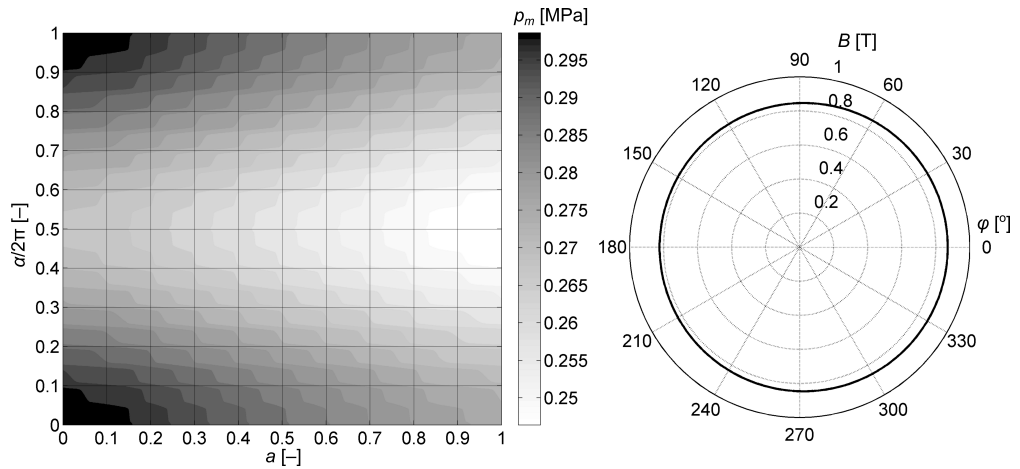


FIG. 5. Magnetic energy density (left) and magnitude of magnetic flux density in the radial air gap for non-slotted armature.

The magnitude of the magnetic flux density over the circumference of the armature varies from 0.83 [T] on the position of the biggest air gap to 0.88 [T] on the smallest (see Fig. 5 on right). The relative magnetic eccentricity is equal  $\varepsilon_m = 2.845$  [%].

After having found the armature eccentricity the equation (5.15) was solved. The obtained distribution of the axial oil velocity at the temperature  $T^{\min}$  is shown in Fig. 6 on the left. One can see that the velocity of the oil film is nearly independent from the circumferential position and falls quite linearly along the hydraulic gap. For the obtained velocity distribution the viscous shear stress vector was found using the relation (5.18). Its amplitude was shown in Fig. 6 on the right. The distribution of the viscous shear stress is strongly dependent on the circumferential position. The reason for this behavior is the relative high value of the relative hydraulic eccentricity. It is equal in this computational case  $\varepsilon_h = 85.350$  [%]. Detailed computation results of both magnetic and hydraulic eccentricity for non-slotted armatures of different radii were recently presented in [22].

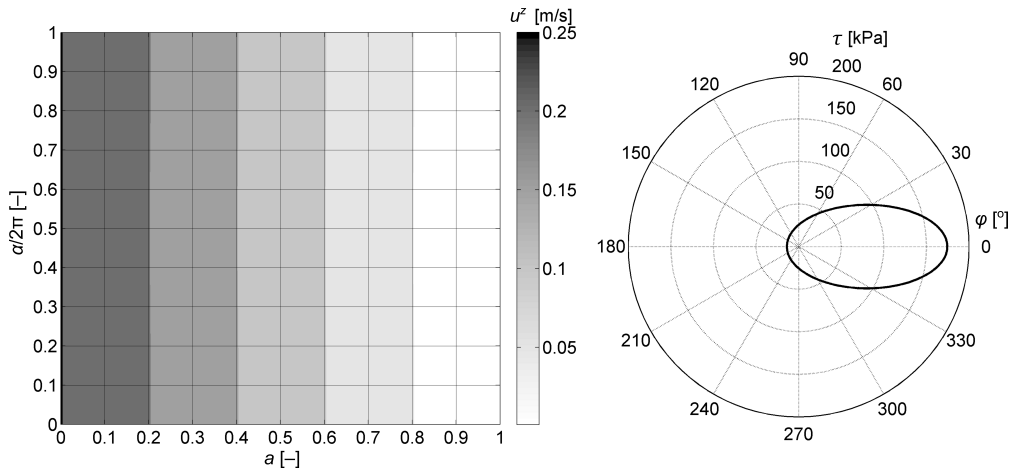


FIG. 6. Axial oil velocity (left) and the magnitude of viscous shear stress vector in the radial oil film at  $T^{\min}$  for non-slotted armature.

The hydraulic results were re-computed for  $T^{\max}$  and shown in Fig. 7. At this temperature one can see a certain dependency of the oil velocity on the circumferential position. The viscous shear stress drops at this temperature mainly because of the lower oil viscosity for almost two powers of ten regarding the temperature  $T^{\min}$ .

Because in the case of  $x$ -axis symmetric contour of the armature the force components  $F_k^y$  and  $F_m^y$  are equal zero, the resulting axial component of the force acting on the armature can be find using the relation (6.1). The relation of the accelerated to the braking force one can find using the relation (6.2).

$$(6.1) \quad \Gamma = F_m^z + F_h^z + F_q^z,$$

$$(6.2) \quad \Omega = -F_m^z (F_h^z + F_q^z)^{-1}.$$

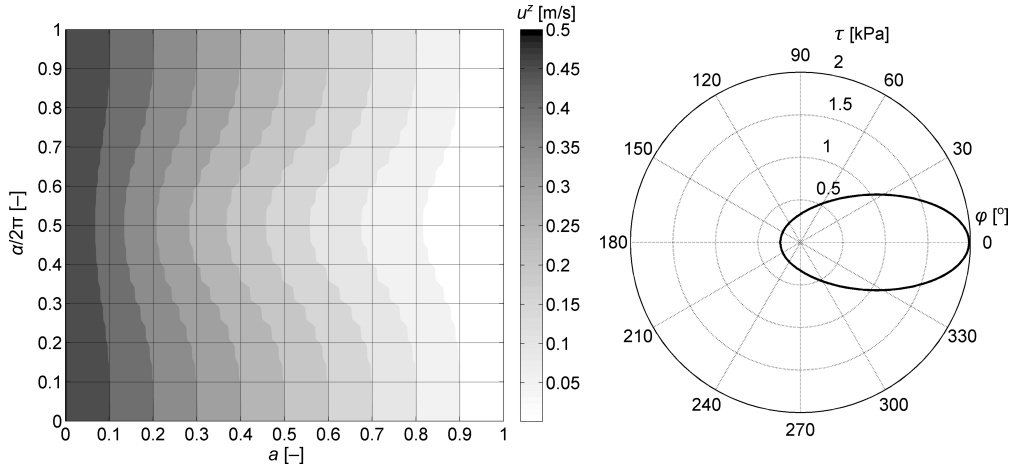


FIG. 7. Axial oil velocity (left) and the magnitude of viscous shear stress vector in the radial oil film at  $T^{\max}$  for non-slotted armature.

In the next step the resulting force as well as the force relation was computed at  $T^{\min}$  and  $T^{\max}$  and for different depth of armature slots according to (2.1). Because of comparison purpose the resulting force as well as the force relation was than normalised by values of non-slotted armature according to (6.3) and (6.4).

$$(6.3) \quad \frac{\Gamma_A}{\Gamma_{A0}} = \frac{\Gamma(\delta, T = T^{\min})}{\Gamma(\delta = 0, T = T^{\min})}, \quad \frac{\Gamma_B}{\Gamma_{B0}} = \frac{\Gamma(\delta, T = T^{\max})}{\Gamma(\delta = 0, T = T^{\max})},$$

$$(6.4) \quad \frac{\Omega_A}{\Omega_{A0}} = \frac{\Omega(\delta, T = T^{\min})}{\Omega(\delta = 0, T = T^{\min})}, \quad \frac{\Omega_B}{\Omega_{B0}} = \frac{\Omega(\delta, T = T^{\max})}{\Omega(\delta = 0, T = T^{\max})}.$$

The computed normalised resulting axial forces (being the function of the depth of the armature slots) were shown in Fig. 8 on the left. The intension of the change of the slots depth was to determine what is an optimal slot depth, that means to determine, for which depth the resulting force and the force relation gets its maximum. For the oil temperature  $T^{\min}$  the introduce of axial slots caused the increase of the resulting axial force up to about 23% regarding the non-slotted armature. However, for the temperature  $T^{\max}$  the increase of the slot depth causes a decrease of the resulting axial force.

The normalised force relations were shown in Fig. 8 on the right. For all the examined range of depths of the slots and independent from the temperature the force relations are bigger than in the case of non-slotted armature. That means that the relation of the accelerating force to the braking forces is getting higher in the case of slotted armatures. High force relation results in the reduction of the friction which degrades the performance of the SV and causes wear.

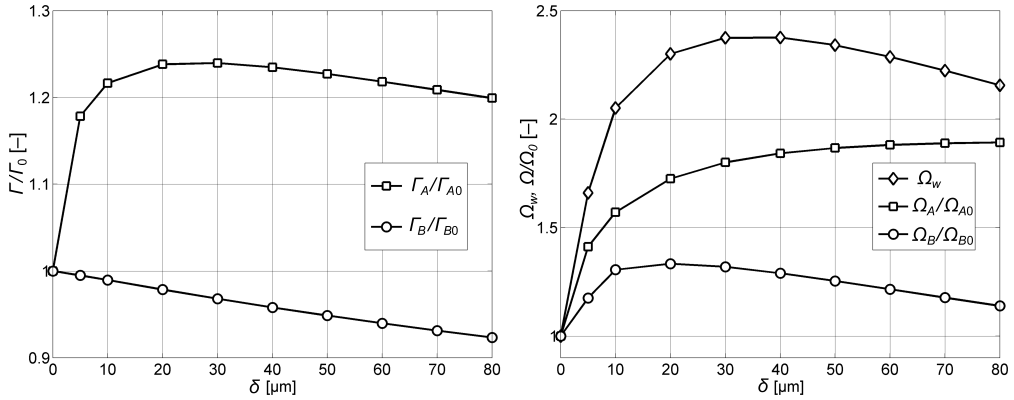


FIG. 8. Normalised resulting axial forces (left) and normalised force relations.

In order to find optimum slot depth the product of normalised force relations (6.5) was built and shown in Fig. 8 on the right.

$$(6.5) \quad \Omega_w = \frac{\Omega_A}{\Omega_{A0}} \frac{\Omega_B}{\Omega_{B0}}.$$

The maximum of  $\Omega_w$  lies at the slot depth of  $\delta = 40 \mu\text{m}$ . For this depth the normalised resulting axial forces are  $\Gamma_A \Gamma_{A0}^{-1} = 1.23$ ,  $\Gamma_B \Gamma_{B0}^{-1} = 0.96$  and the normalised force relations are  $\Omega_A \Omega_{A0}^{-1} = 1.84$ ,  $\Omega_B \Omega_{B0}^{-1} = 1.29$ . The introduction of axial slots resulted in the inhomogeneous distribution of the magnitude of the magnetic flux density over the armature circumference caused by the local change of the radial air gap (see Fig. 9).

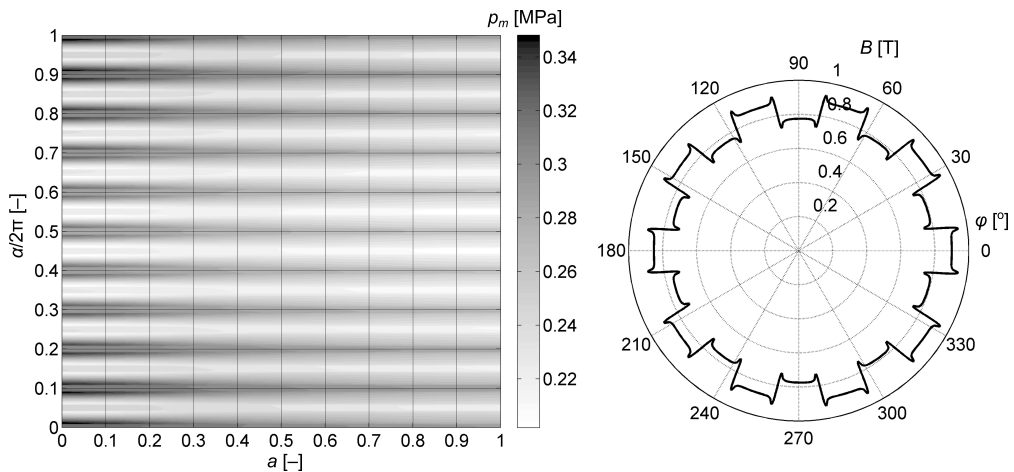


FIG. 9. Magnetic energy density (left) and magnitude of magnetic flux density in the radial air gap for armature with the slot depth equal  $40 \mu\text{m}$ .

Because of this distribution the armature is less attracted to the sleeve what results in the decrease of the dry friction force (5.13). On the other hand however the slots cause bigger drop of the magnetomotive force in the radial air gap and simultaneous decrease of the armature cross section area  $A_d$ . These two facts have a direct impact of the decrease of the magnetic driving force  $F_m^z$ .

From the hydraulic point of view however the slots influence much the viscous shear stress. One can see from the Fig. 10 a significant drop of the magnitude of the viscous shear stress vector on the circumferential position of each slot.

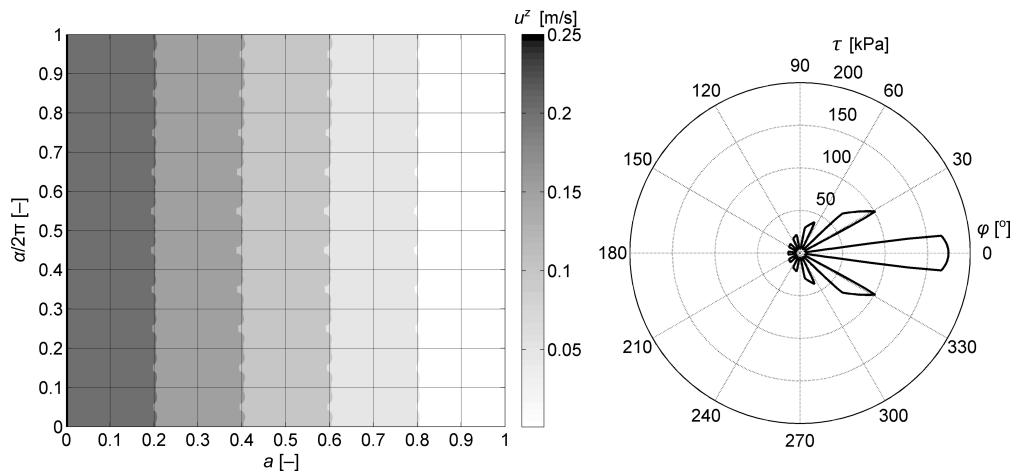


FIG. 10. Axial oil velocity (left) and the magnitude of viscous shear stress vector in the radial oil film at  $T^{\min}$  for armature with the slot depth equal  $40 \mu\text{m}$ .

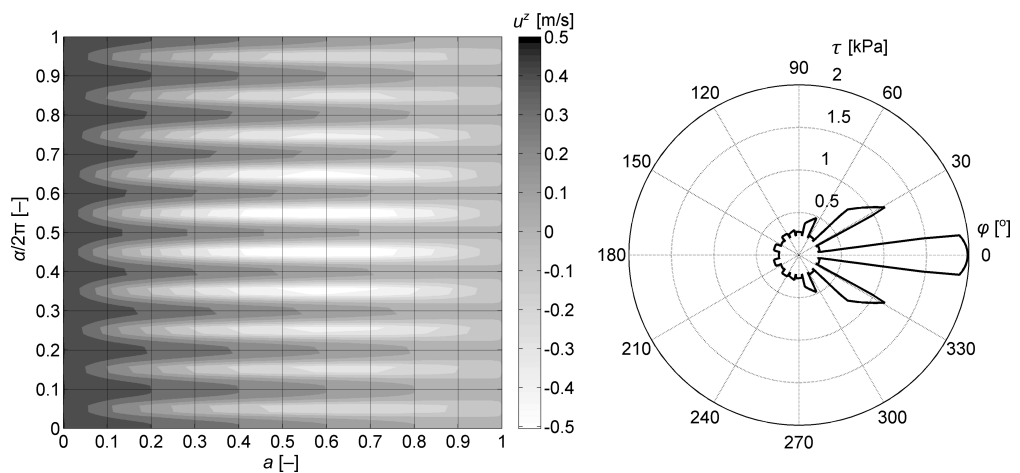


FIG. 11. Axial oil velocity (left) and the magnitude of viscous shear stress vector in the radial oil film at  $T^{\max}$  for armature with the slot depth equal  $40 \mu\text{m}$ .

Finally the normalised force  $\Gamma_A \Gamma_{A0}^{-1}$  reaches at temperature  $T^{\min}$  values bigger one.

One can see a similar distribution of the magnitude of the viscous shear stress also at the temperature  $T^{\max}$  (Fig. 11). At his temperature however the contribution of the viscous friction force to the resulting axial force  $\Gamma$  is – because of the oil viscosity – much lower than at  $T^{\min}$ . Finally the normalised force  $\Gamma_B \Gamma_{B0}^{-1}$  falls at temperature  $T^{\max}$  below one.

## 7. CONCLUSIONS AND FURTHER RESEARCH STEPS

- Introduction of ten axial slots with the depth 40  $\mu\text{m}$  in the armature increased in the investigated SV the driving force of 23% at the temperature of  $-10^\circ\text{C}$  and declined it of 4% at the temperature of  $140^\circ\text{C}$ .
- At the temperature of  $-10^\circ\text{C}$  as well as at the temperature of  $140^\circ\text{C}$  the axial slots increase the ratio of the accelerating (magnetic) force to the braking (friction) force. This increase has a positive impact of the wear of SV.
- By means of a randomly chosen number of axial slots it could be computationally proved that the insertion of small axial slots in the armature of SV has a beneficial technical effect on the increase of the performance of SV.
- In order to approach the question what is an optimal number of axial slots, optimal peripheral length of the slots and their optimal depth further investigation as well as measured verifications are required.

## REFERENCES

1. GORAJ R., *Impact of the pulse width modulation on the temperature distribution in the armature of the solenoid valve*, International Journal of Applied Mechanics and Engineering, **20**(4): 773–786, 2015.
2. VOGEL R., *Numerical calculation of the armature friction of an electromagnetic switching valve*, Studies work [in German], Universität Dortmund, Dortmund, 2006.
3. DELAND D.L., *Solenoid arrangement with segmented armature member for reducing radial force*, Davison, MI (US) Patent US 8,421,568 B2, 16 April 2013.
4. GORAJ R., *Electromagnetic switching valve* [in German], German Patent DE 10 2007 023 363 A1, 18 May 2007.
5. BOTTAUSCIO O., CHIAMPI M., MANZIN A., *Different finite element approaches for electromechanical dynamics*, IEEE Transactions on Magnetics, **40**(2): 541–544, 2004.
6. PENG L., LIYUN F., QAISAR H., DE X., XIUZHEN M., ENZHE S., *Research on key factors and their interaction effects of electromagnetic force of high-speed solenoid valve*, The Scientific World Journal, Hindawi Publishing Corporatio, Article ID 567242, 2014.

7. ANGADI S.V., JACKSON S., CHOE S., *Reliability and life study of hydraulic solenoid valve. Part 1: A multi-physics finite element model*, Engineering Failure Analysis, **16**(3): 874–887, 2009.
8. EPSTEIN M., *Differential geometry, basic notions and physical examples*, Springer, 2014.
9. MCINERNEY A., *First steps in differential geometry, Riemannian, contact, symplectic*, Springer, New York, 2013.
10. NGUYEN-SCHÄFER H., SCHMIDT J.-P., *Tensor analysis and elementary differential geometry for physicists and engineers*, Springer, Berlin, Heidelberg, 2014.
11. GORAJ R., *Re-derivation of Laplace operator on curvilinear coordinates used for the computation of force acting in solenoid valves*, Journal of Applied Mathematics and Computational Mechanics, **15**(1): 25–38, 2016.
12. GETZLAFF M., *Fundamentals of magnetism*, Springer, Berlin, Heidelberg, 2008.
13. RAWA H., *Electricity and magnetism in technology* [in Polish], Wydawnictwo Naukowe PWN, Warszawa, 2001.
14. KÜPFMÜLLER K., KOHN G., *Theoretical electrical engineering and electronics* [in German], Springer, Berlin, 1993.
15. STEFANITA C.-G., *Magnetism, basics and applications*, Springer, Berlin, Heidelberg, 2012.
16. KALLENBACH E., EICK R., QUENDT P., STRÖHLA T., FEINDT K., KALLENBACH M., RADLER O., *Electromagnets basics, calculation, design and application* [in German], Teubner Verlag/GWV Fachverlage GmbH, Wiesbach, 2003.
17. GREENWOOD J., WILLIAMSON J., *Contact of nominally flat surfaces*, Proceedings of The Royal Society. A: Mathematical Physical and Engineering Sciences, **295**: 300–319, 1966.
18. KLEIST A., *Calculation of sealing and bearing joints in hydrostatic machines* [in German], Shaker Verlag, Aachen, 2002.
19. PUZYREWSKI R., SAWICKI J., *Fundamentals of fluid mechanics and hydraulics* [in Polish], Wydawnictwo Naukowe PWN, Warszawa, 2000.
20. GRYBOŚ R., *Exercises in the technical mechanics of fluids* [in Polish], Wydawnictwo Naukowe PWN, Warszawa, 2002.
21. LANDAU L., LIFSHITZ E., *Fluid mechanics. Course of theoretical physics. Vol. 6*, Pergamon Press, 1966.
22. GORAJ R., *Impact of the sleeve thickness on the armature eccentricity in a solenoid valve*, Archives of Electrical Engineering, **65**(2): 371–382, 2016.

*Received December 21, 2015; accepted version July 12, 2016.*

---